PCCP

ROYAL SOCIETY OF CHEMISTRY

PAPER

Cite this: *Phys. Chem. Chem. Phys.*, 2023, **25**, 3083

Theoretical vibrational mode-specific dynamics studies for the HBr + C_2H_5 reaction

Cangtao Yin * and Gábor Czakó *

A quasi-classical trajectory (QCT) study is performed for the HBr + C_2H_5 multi-channel reaction using a recently-developed high-level *ab initio* full-dimensional spin–orbit-corrected potential energy surface (PES) by exciting five different vibrational modes of reactants at five collision energies. The effect of the normal-mode excitations on the reactivity, the mechanism, and the post-reaction energy flow is followed. A significant decrease of the reactivity caused by the longer initial distances of the reactants for the v_{HBr} = 1 reaction at low collision energy (E_{coll}) is observed due to the intramolecular vibrational-energy redistribution and the classical nature of the QCT method. All of the three reaction pathways (H-abstraction, Br-abstraction, and H-exchange) are intensely promoted when the HBr-stretching mode is excited. No clear promotion is observed when excitation is imposed to C_2H_5 except that asymmetric CH-stretching helps the H-exchange process. The enhancement effect of the excitation in the HBr vibrational mode is found to be much more effective than increasing the translational energy, in contrast to the HBr + CH_3 reaction. The forward scattering mechanism can be clearly promoted by the excitation of the HBr-stretching mode, or by the high collision energy, indicating the dominance of the direct stripping mechanism in these cases. At low collision energy with no excitation or excitation of any vibrational mode of C_2H_5, the forward scattering feature is less obvious. At E_{coll} = 1 kcal mol^{-1}, when HBr-stretching is excited, the product clearly gains more relative translational energy. However, it is interesting to see that when the excitation is in C_2H_5, the effect is the opposite, *i.e.*, the product gains less relative translational energy compared to the ground-state reaction.

Received 14th November 2022,
Accepted 15th December 2022

DOI: 10.1039/d2cp05334a

rsc.li/pccp

I. Introduction

The reactions of hydrogen-bromide with alkyl radicals (HBr + R → Br + RH) have been the subject of both theoretical and experimental investigations, and are also used to determine the heats of formation of radicals and C–H bond energies. The experimental study of the kinetics and thermochemistry for these reactions includes laser photolysis/time-resolved infrared chemiluminescence,[1] tubular reactor coupled to photoionization mass spectrometry,[2] time-resolved resonance fluorescence,[3] excimer laser flash photolysis coupled with photoionization mass spectrometry,[4] a heatable tubular reactor,[5,6] excimer laser photolysis-transient UV spectroscopy,[7] and single-photon photoionization mass spectrometry.[8,9] The rate coefficients for the reaction determined by the above different groups and by different experimental techniques provided negative activation energies for these reactions within their temperature range.

From the theoretical side, the prototype of this class of reaction, HBr + CH_3 → Br + CH_4, has been extensively studied in detail. Chen *et al.*[10] located the minimum and transition state of the reaction and further investigated the rate constants by RRKM and G1 theory.[11] The thermal rate coefficients calculated by Yu and Nyman[12] show a strong nonlinear Arrhenius behavior. Below 550 K they have a negative temperature dependence, whereas a positive activation energy was obtained at higher temperatures. They also found that placing one quantum of energy in the vibrational mode of the H–Br bond stretch enhances the reactivity, whereas one quantum in the umbrella mode of CH_3 has the opposite effect. Espinosa-Garcia[13] calculated the forward and reverse thermal rate constants and the kinetic isotope effects using variational transition state theory with semiclassical transmission coefficients over a wide temperature range. The theoretical rate constants provided by Sheng *et al.*[14] using improved canonical variational transition state theory incorporating small-curvature tunneling correction are in excellent agreement with the experimental values. Krasnoperov[15] developed a modified transition state theory for gas-phase reactions with negative barriers and applied it to the reaction HBr + CH_3. Wang *et al.*[16] showed that the individual excitation of the CH_3 symmetric stretching mode,

MTA-SZTE Lendület Computational Reaction Dynamics Research Group, Interdisciplinary Excellence Centre and Department of Physical Chemistry and Materials Science, Institute of Chemistry, University of Szeged, Rerrich Béla tér 1, Szeged H-6720, Hungary. E-mail: cangtaoyin@foxmail.com, gczako@chem.u-szeged.hu

the umbrella mode and the HBr stretching mode visibly enhances the reaction while they are all less efficient than the translational energy in promoting the reaction, as expected for an early-barrier reaction. In 2013, one of us[17] developed a high-quality full-dimensional PES for the backward Br + CH_4 reaction based on CCSD(T)/aug-cc-pwCVTZ-PP-quality *ab initio* energy points. Later a new version was developed[18] by calculating the potential energy at the same *ab initio* level at 5000 additional geometries in the region of CH_3 + HBr van der Waals potential well, and the rate coefficients were determined by QCT calculations. Using the same PES, the integral cross sections were calculated by both a six-degree-of-freedom reduced-dimensional quantum dynamics and the QCT method and very good agreement was found between the two approaches.[19] The cross sections were found to diverge when the collision energy decreases, indicating that the reactant attraction is responsible for the dynamics at low collision energy. The quantum mechanical and the quasi-classical rate constants also agree very well and almost exactly reproduce the experimental results at low temperatures up to 540 K.

For the HBr + C_2H_5 reaction, however, only a small amount of theoretical work has been done, including the evaluation of absolute rate constants and kinetic isotope effects by transition state theory and RRKM theory,[20] the calculation of the enthalpy of formation,[21] the determination of the temperature dependence over the temperature range from 200 to 1400 K,[22] and the analysis of the kinetics by employing RRKM theory.[23] The computed rate constants agree well with most experimental data in the literature, and indicate that at temperatures above 850 K, the activation energy may switch from negative to positive.

In 2019 our group[24] determined benchmark geometries and energies for the stationary points of the backward reaction Br + C_2H_6, considering also the H-substitution and the methyl-substitution reaction pathways, by augmenting the CCSD(T)-F12b/aug-cc-pVQZ energies with core-correlation, post-CCSD(T) and spin–orbit corrections. Taking these correction terms into account turns out to be essential to reach subchemical, *i.e.* 0.5 kcal mol^{-1}, accuracy. Very recently[25] we reported a high-level *ab initio* full-dimensional spin–orbit-corrected PES built from 11 364 geometries and energies at the following composite level of theory: ManyHF-based[26] UCCSD(T)-F12a/cc-pVDZ-F12 (-PP) + SO_{corr}(MRCI-F12+Q(5,3)/cc-pVDZ-F12),[27] where for the Br atom a small-core relativistic effective core potential (ECP)[28] is used. The multi-reference computations utilized a minimal active space of 5 electrons on 3 spatial 4p-like orbitals, and the Q Davidson-correction[29] estimates higher-order correlation energy effects. The SO computations made use of the Breit–Pauli operator in the interacting-states approach,[30] where the SO eigenstates were determined by diagonalizing the 6 × 6 SO matrix whose diagonal elements were replaced by the Davidson-corrected MRCI energies. For the fitting of the energy points of the PES we utilized the Monomial Symmetrization Approach (MSA).[31] The ground-state dynamics for the HBr + C_2H_5 → $Br(^2P_{3/2})$ + C_2H_6 reaction were also studied in that work. With the purpose of providing more accurate dynamical and mechanistic descriptions, and aiming to achieve the ultimate goal of explaining the temperature dependence of the rate constant behavior, here we investigate the competition between vibrational and translational excitation in the nine-atomic reaction featuring an early barrier slightly submerged below the reactants. The HBr-stretching mode and four selected vibrational modes of the ethyl radical are excited, one at a time and each with one quantum, at five different collision energies. The effects of the different kinds of excitations on the reactivity, the reaction mechanisms, the alternative product channels, and the post-reaction distribution of energy are monitored.

II. Methodology

A. Quasi-classical trajectory

QCT simulations are carried out at collision energies (E_{coll}) of 1, 5, 10, 20, and 40 kcal mol^{-1} for the HBr + C_2H_5 reaction on the full-dimensional spin–orbit-corrected PES recently developed by the present authors.[25] Clearly the HBr-stretching excitation is expected to promote the reaction most efficiently. For the ethyl radical, the vibrational mode from the CH_2 part should be more important than CH_3 part. Therefore, we pick the HBr-stretching and four different ethyl normal mode (from CH_2 part) excitations, each with one quantum [the ν_{HBr} HBr-stretching (7.65), the ν_9 CH_2 wagging (1.08), the ν_5 CH_2 bending (4.15), the ν_1 symmetric CH-stretching (9.20), and the ν_{10} asymmetric CH-stretching (9.37) modes with fundamental harmonic energies given in kcal mol^{-1} in parentheses], and compare the results with those obtained for the ground-state reaction. The motions corresponding to these normal-mode vibrations of ethyl are represented in Fig. 1.

At the beginning of the trajectories, the initial vibrational excitation energies and the zero-point energies (ZPEs) of HBr and C_2H_5 are set by standard normal-mode sampling.[32] The spatial orientations of the reactants are randomly sampled. The initial distance between the center of mass of HBr and the center of mass of C_2H_5 is $(x^2 + b^2)^{1/2}$, where x = 16 bohr and the impact parameter is varied between 0 and b_{max} (where the reaction probability vanishes) with a step size of 0.5 bohr. Note that the x-dependence of the reactivity is also studied as described in Section III A. 1000 trajectories are run at each b value. The trajectories are propagated with a 0.0726 fs time step until the largest interatomic distance becomes larger than the largest initial one by 1 bohr.

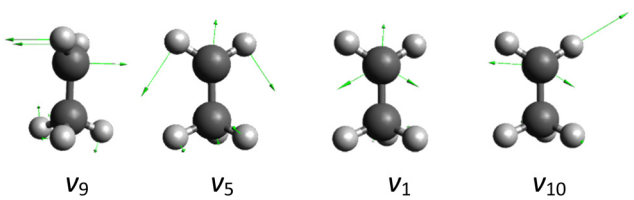

Fig. 1 Schematic representation of the normal-mode vibrations of ethyl studied in the present work: ν_9 CH_2 wagging, ν_5 CH_2 bending, ν_1 symmetric CH-stretching, and ν_{10} asymmetric CH-stretching, where ν_x [x = 9, 5, 1, 10] refer to the standard Mulliken notations.

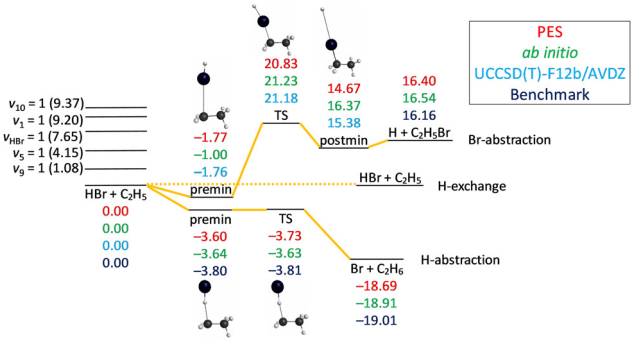

Fig. 2 Schematic potential energy diagram of the HBr + C_2H_5 reaction comparing the classical relative energies obtained on the PES, ManyHF-UCCSD(T)-F12a/cc-pVDZ-F12 + SO_{corr}(MRCI-F12+Q(5,3)/cc-pVDZ-F12(-PP)) energies at geometries optimized on the PES, UCCSD(T)-F12b/AVDZ relative energies at geometries optimized at UCCSD(T)-F12b/AVDZ or the relativistic all-electron CCSDT(Q)/complete-basis-set-quality benchmark relative energies[24] of the stationary points. Five single-excited vibrational energy levels (in parentheses) of the reactants obtained on the PES are also shown. All the energies are given in kcal mol^{-1}.

Integral cross sections (σ) for the HBr + C_2H_5 reaction are calculated by a b-weighted numerical integration of the $P(b)$ opacity functions at each E_{coll}. The product ZPE-constraint, *i.e.*, the classical vibrational energy of C_2H_6 has to be greater than its ZPE on the present PES, only rules out 8/4/3 trajectories from the 5793/4840/8555 reactive trajectories of no/v_9/v_{HBr} excitation. So from now on we can safely ignore the differences between the features with and without ZPE constraints. The scattering angle distributions are obtained by binning the cosine of the angle (θ) of the relative velocity vectors of the center of masses of the products and those of the reactants into 10 equidistant bins from −1 to 1. $\cos(\theta) = 1$ ($\theta = 0^\circ$) corresponds to forward scattering and $\cos(\theta) = -1$ ($\theta = 180^\circ$) corresponds to backward scattering. The initial attack angle distributions for the reactants are calculated by binning the cosine of the angle (α for HBr and β for C_2H_5) of the velocity vector of the center of mass of the examined reactant and an interatomic vector that is considered as the Br–H bond for HBr and the C–C bond for C_2H_5. We also use 10 equidistant bins between −1 to 1 like for the scattering angle distributions. For HBr $\cos(\alpha) = -1$ means that HBr approaches with its Br atom side and in the situation of $\cos(\alpha) = 1$ HBr goes with its H atom towards C_2H_5. While for C_2H_5 $\cos(\beta) = -1$ means that C_2H_5 approaches HBr with its CH_3 side and in the situation of $\cos(\beta) = 1$ C_2H_5 goes with its CH_2 side towards the HBr. The rotational quantum numbers of the C_2H_6 product are obtained by rounding the lengths of the classical rotational angular momentum vectors, in atomic units, to the nearest integer values.

B. Potential energy surface

The schematic energy diagram of the title reaction is shown in Fig. 2. We have identified three reaction pathways of the HBr + C_2H_5 reaction: H-abstraction HBr + C_2H_5 → Br + C_2H_6, Br-abstraction HBr + C_2H_5 → H + C_2H_5Br, and H-exchange H′Br + C_2H_5 → HBr + C_2H_4H'. For the last one there are at least two sub-pathways: bromine may take a hydrogen from CH_2 or from CH_3, and these are probably multi-step mechanisms (not shown in Fig. 2). As we will see in the next section, the latter two reaction pathways only contribute less than 1% of the total reaction, except in the case of the excitation of HBr-stretching when their contribution is about 3.5%. So we will mainly focus on H-abstraction except in the integral cross section analysis. For the H-abstraction reaction pathway, a pre-reaction minimum is located very near to the submerged transition state (TS) and the reaction is exothermic. For the Br-abstraction reaction pathway, both the pre-reaction minimum and the post-reaction minimum are located below the corresponding reactants and products. The TS is about 21 kcal mol^{-1} with respect to the reactants and the reaction is endothermic. Fig. 2 also shows the comparison of the classical relative energies of the stationary points of the HBr + C_2H_5 reaction obtained on the analytical PES, the ManyHF-UCCSD(T)-F12a/cc-pVDZ-F12 + SO_{corr}(MRCI-F12+Q(5,3)/cc-pVDZ-F12(-PP)) energies computed at the geometries optimized on the PES, and the previously determined benchmark results (where available).[24] The comparison of the former two indicates excellent fitting behavior for the H-abstraction reaction pathway but only just good fitting behaviour for the Br-abstraction reaction pathway, as the PES was designed for describing the hydrogen-abstraction pathway.[25]

III. Results and discussion

A. Initial distance

In our previous work[25] we used a longer initial distance between HBr and C_2H_5 $r = (x^2 + b^2)^{1/2}$, where x = 28 bohr. At low E_{coll} for larger r there is more time for intramolecular vibrational-energy redistribution (IVR) prior to collision. It may influence the QCT result, especially in the excited-state reaction with low collision energy. To investigate the effect of the initial distance on the QCT results, we tested 500 trajectories with x = 28 and 16 bohr at $b = 0 - b_{max}$ with a step size of 1 bohr, for the ground-state and

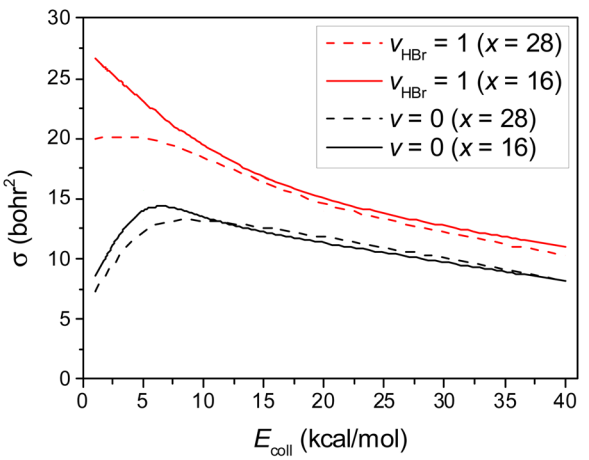

Fig. 3 Initial distance dependence of the integral cross sections for the HBr(v_{HBr} = 0, 1) + C_2H_5(v = 0) → Br + C_2H_6 reactions as a function of collision energy, where the initial distance between the center of mass of HBr and the center of mass of C_2H_5 is $(x^2 + b^2)^{1/2}$, with x = 16 and 28 bohr.

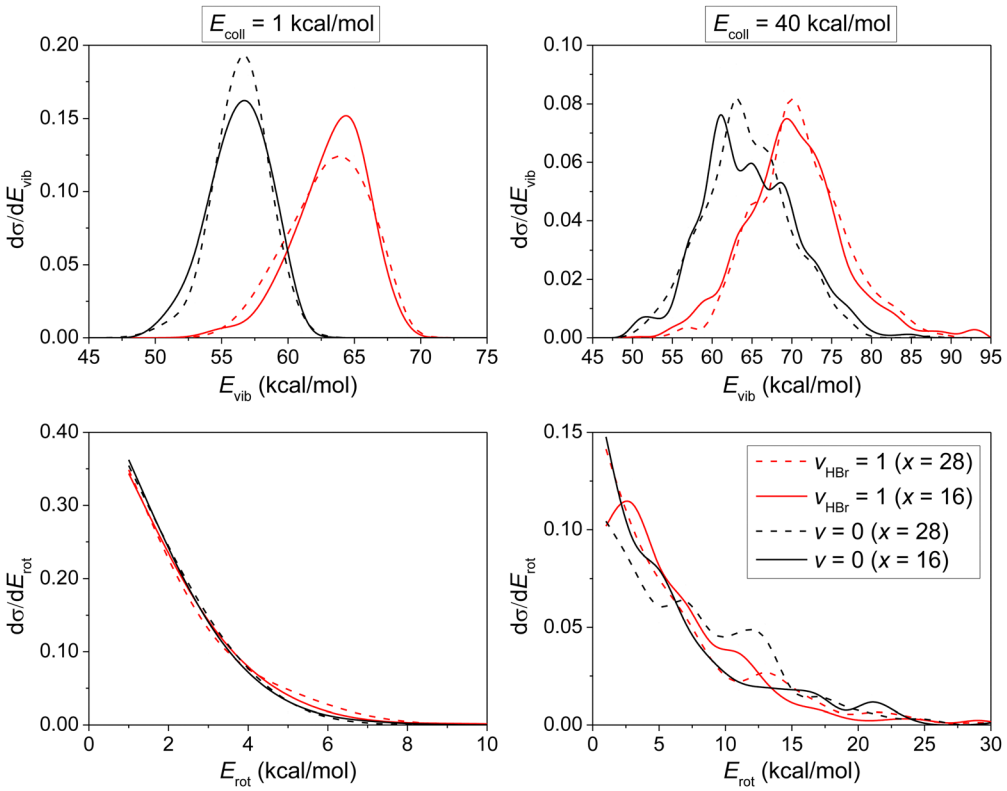

Fig. 4 Initial distance dependence of the normalized vibrational energy (E_{vib}) and rotational energy (E_{rot}) distributions for the product ethane of the HBr(v_{HBr} = 0, 1) + C_2H_5(v = 0) → Br + C_2H_6 reaction at different collision energies, where the initial distance between the center of mass of HBr and the center of mass of C_2H_5 is $(x^2 + b^2)^{1/2}$, with x = 16 and 28 bohr.

v_{HBr} = 1 reactions. The integral cross sections (σ) as a function of E_{coll} of the HBr + C_2H_5 reaction, presented in Fig. 3, show a significant decrease for the v_{HBr} = 1 reactivity at low E_{coll} when we increase the initial distance, *i.e.*, increase the time for IVR. As E_{coll} increases, the chance of IVR is less and the cross sections become similar with x = 28 and 16 bohr. In the case of the ground-state reaction the cross sections do not show a significant initial distance dependence, and only a small reactivity decrease with increasing distance is found at low E_{coll}. Note the classical IVR can happen even at the vibrational ground state, and the classical IVR in C_2H_5(v = 0) may affect the v_{HBr} = 0 and v_{HBr} = 1 reactions differently, as we have found.

Differential cross sections showing the initial distance dependence of the vibrational and rotational energy distributions of the product ethane from the HBr + C_2H_5 → Br + C_2H_6 reaction are plotted in Fig. 4.

From Fig. 4 we see that the longer initial distance between reactants only has a minor influence on the post-reaction energy distribution, both in the ground state and excited cases. Thus, these test computations show that the choice of the initial distance did not have any significant effect on our previous results for the ground-state reaction. In the present mode-specific study we use the shorter initial distance (x = 16 bohr) to decrease the time for IVR prior to collision,

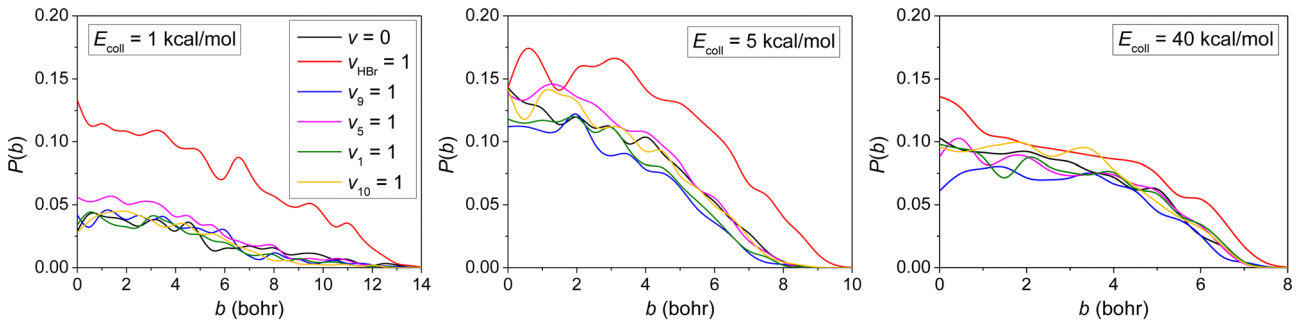

Fig. 5 Reaction probabilities as a function of the b impact parameter for the HBr(v_{HBr} = 0, 1) + C_2H_5(v_x = 0, 1) → Br + C_2H_6 [x = 9, 5, 1, 10] reactions at different collision energies.

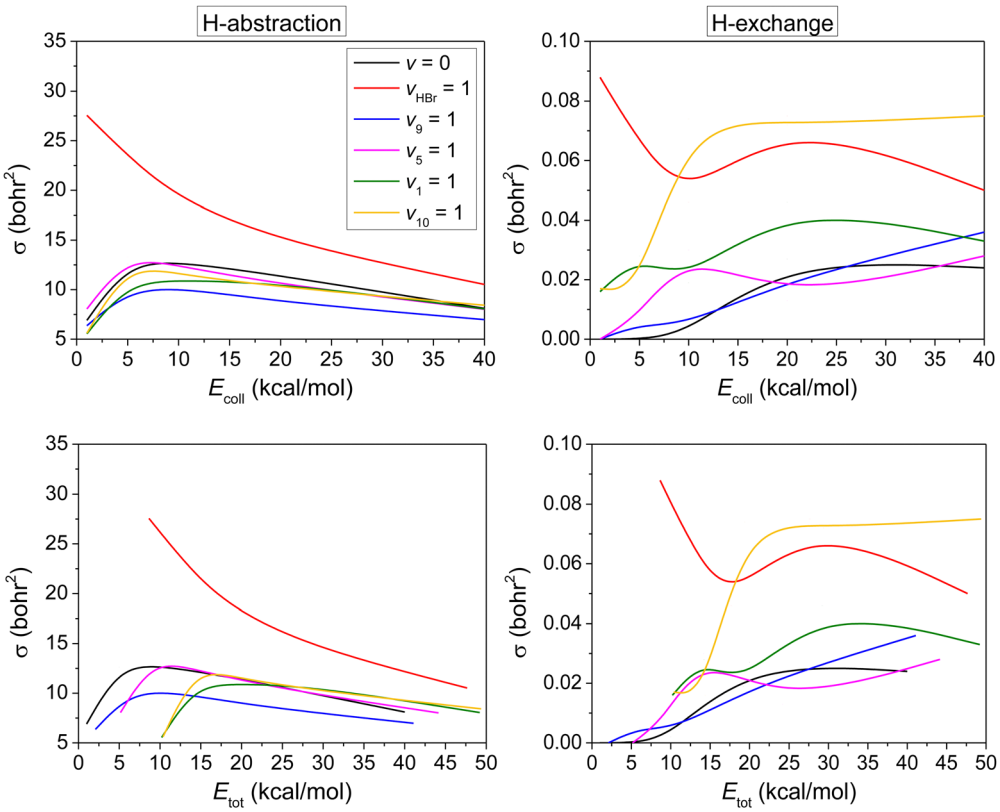

Fig. 6 Integral cross sections as a function of collision energy (upper panels) and total energy (lower panels) for the HBr(v_{HBr} = 0, 1) + C_2H_5(v_x = 0, 1) [x = 9, 5, 1, 10] H abstraction and exchange reactions.

which may affect the cross sections at low E_{coll} as we have just demonstrated. Finally, we emphasize that IVR in the isolated reactants occurs in every QCT study due to classical mechanics and the anharmonic nature of the PES (see, for example, ref. 33, where mode energies of isolated C_2H_6 as a function of time are examined). This IVR does not necessarily indicate any problem with the PES. For the title reaction the correct asymptotic behavior of the PES is shown in ref. 25.

B. Reaction probabilities

The opacity functions (reaction probabilities as a function of the impact parameter) of HBr(v_{HBr} = 0, 1) + C_2H_5(v_x = 0, 1) → Br + C_2H_6 [x = 9, 5, 1, 10] reactions obtained at the different E_{coll} are shown in Fig. 5.

As inspecting the opacity functions shown in Fig. 5, we can observe a significant enhancement for the HBr + C_2H_5 → Br + C_2H_6 reaction when v_{HBr} = 1, especially at low collision energy, while the b_{max} values do not change considerably, and the shape of the opacity functions remain, *i.e.*, the reaction probabilities decrease monotonically with increasing b. Only a minor mode-specificity is seen for the four selected vibrational mode excitations of the ethyl radical.

C. Integral cross sections

The integral cross sections (σ) as a function of E_{coll} of the hydrogen-abstraction (HBr + C_2H_5 → Br + C_2H_6) and hydrogen-exchange (H′Br + C_2H_5 → HBr + C_2H_4H′) reactions, presented in the upper panel of Fig. 6, reflect a substantial jump for v_{HBr} = 1 in both cases and for v_{10} = 1 (asymmetric CH-stretching) in H-exchange at high E_{coll}, but a reflect a slight inhibition effect or no effect for other mode-specific excitations, which is similar for the HBr + CH_3 reaction in which the excitation of HBr-stretching enhances the reactivity, and the excitation of the umbrella mode of CH_3 has the opposite effect.[12] We checked the trajectories and found out that there are at least three possible different pathways for the H-exchange process. All of the them start with a hydrogen transfer from HBr to ethyl followed by (1) a complex formation, where bromine forms two bonds with two hydrogens of one common carbon, and later Br abstracts one of these H atoms, (2) bromine forming two bonds with two hydrogens of two different carbon atoms before abstracting one of the hydrogens forming an HBr product, and (3) the Br atom moving away from ethane, but the fragments cannot separate, instead Br turns back and abstracts an H atom from ethane. It makes sense that asymmetric CH-stretching helps the H-exchange process, as it increases the possibility of pathways 1 and 3 by facilitating the CH bond cleavage. It is interesting to see that v_9 = 1 (CH_2 wagging) inhibits the hydrogen abstraction quite obviously, because this wagging prevents HBr approaching the CH_2 group.

We also plot the ICS values as a function of the total initial energy in the lower panels of Fig. 6. It gives us better vision that

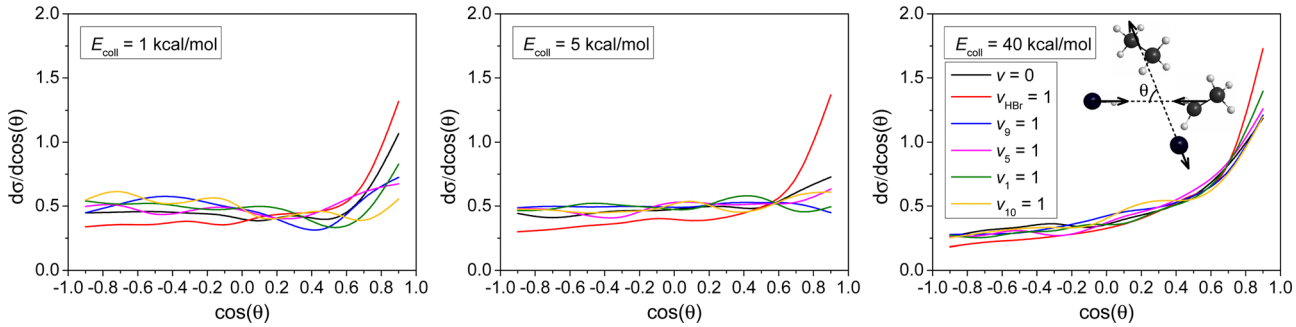

Fig. 7 Normalized scattering angle distributions for the HBr(v_{HBr} = 0, 1) + C_2H_5(v_x = 0, 1) → Br + C_2H_6 [x = 9, 5, 1, 10] reactions.

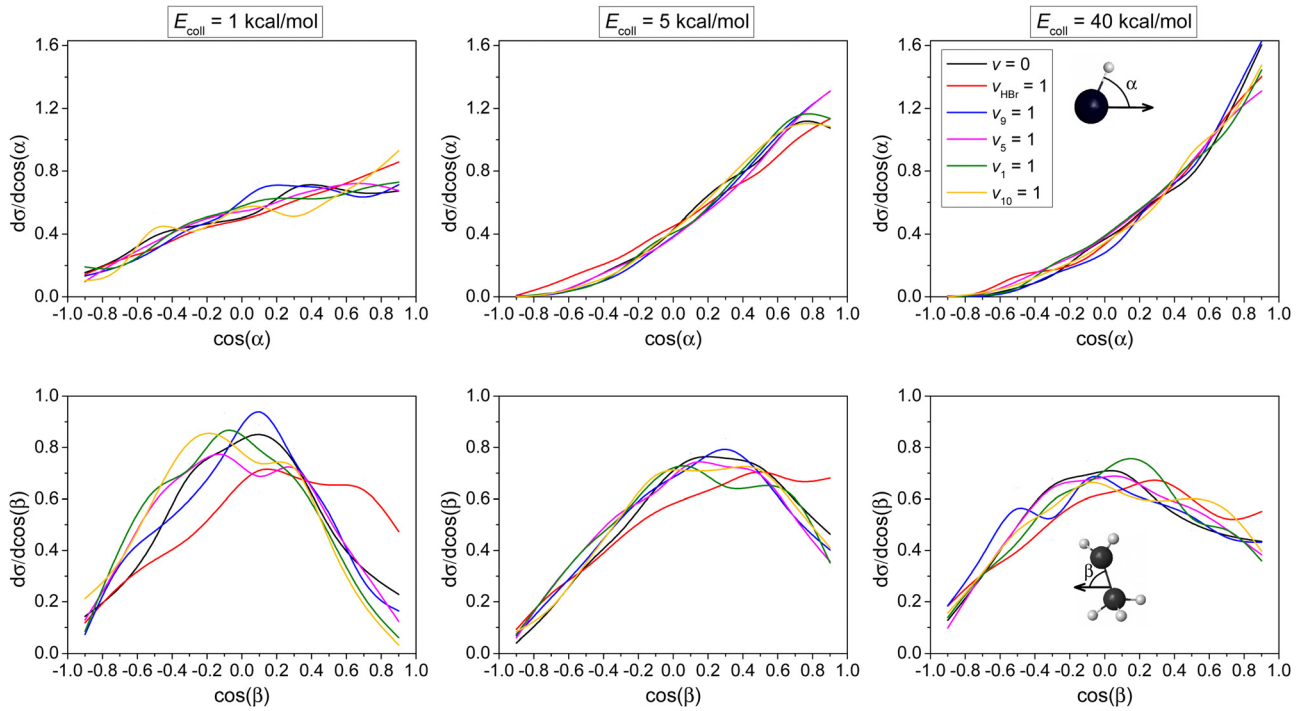

Fig. 8 Normalized initial attack angle distributions for the HBr(v_{HBr} = 0, 1) + C_2H_5(v_x = 0, 1) → Br + C_2H_6 [x = 9, 5, 1, 10] reactions. The attack angles are defined at the beginning of each reactive trajectory. α and β are calculated by the velocity vector of center of mass of the examined reactant and an interatomic vector that is considered as the Br–H bond for HBr and the C–C bond for C_2H_5, respectively.

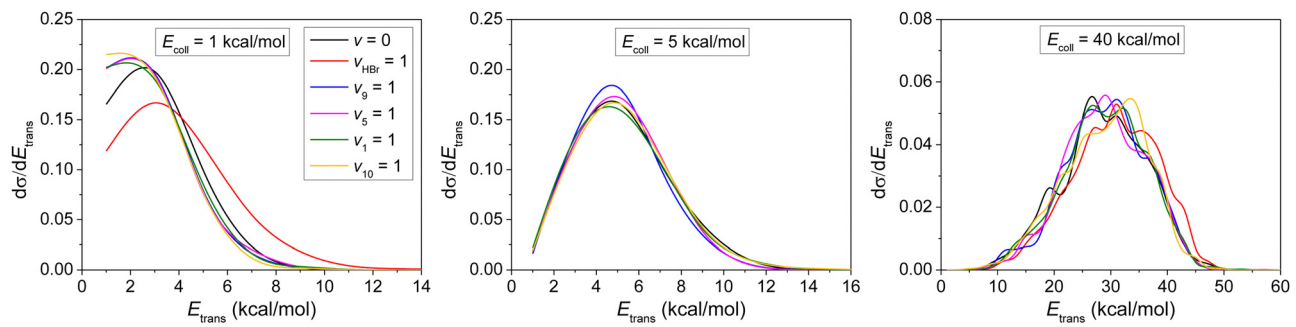

Fig. 9 Normalized product relative translational energy distributions for the HBr(v_{HBr} = 0, 1) + C_2H_5(v_x = 0, 1) → Br + C_2H_6 [x = 9, 5, 1, 10] reactions.

the vibrational excitation of HBr-stretching wins over the effect of increasing translational energy. However, it is not like the case for the HBr + CH_3 reaction, where the vibrational excitation is less efficient than the translational energy.[16]

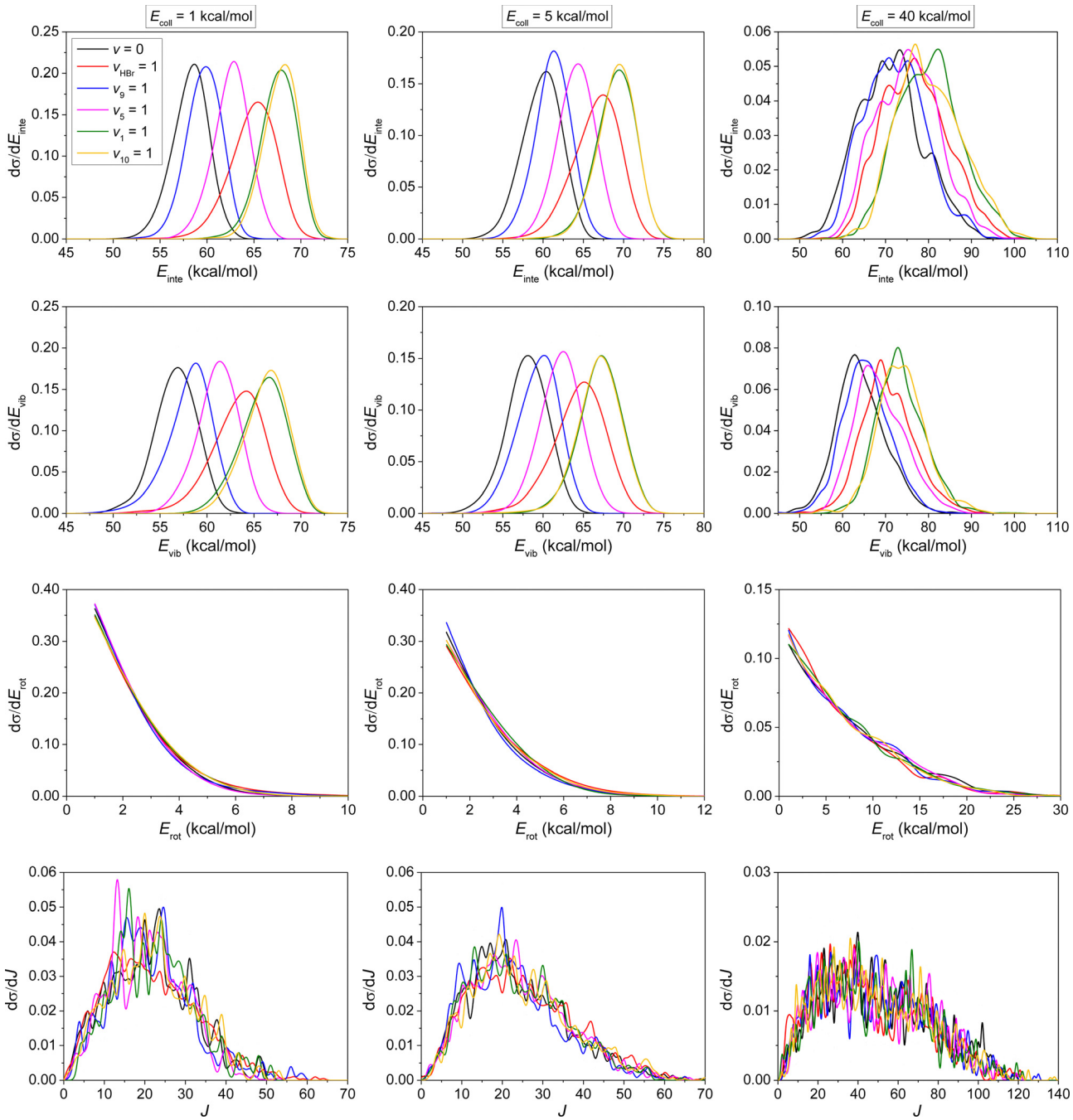

Fig. 10 Normalized internal energy (E_{inte}), vibrational energy (E_{vib}), rotational energy (E_{rot}), and rotational quantum number (J) value distributions for the product ethane for the HBr(v_{HBr} = 0, 1) + C_2H_5(v_x = 0, 1) → Br + C_2H_6 [x = 9, 5, 1, 10] reactions.

From Fig. 6 we can also make a reasonable prediction that the H-exchange reaction barrier is not high, probably less than 5 kcal mol^{-1}. However, the hydrogen exchange pathway contribution is still very small. The largest contribution studied in this work belongs to v_{10} = 1 at E_{coll} = 40 kcal mol^{-1}, which is 0.88%, *i.e.* less than 1/100 compared to the dominant hydrogen-abstraction pathway. This is partly because it is a multi-step reaction, and partly because during the reaction process, in most cases the bromine takes the same hydrogen that it originally carries, and in these cases it does not count as a reaction.

Cross sections for the bromine-abstraction reaction pathway are not plotted here. As can be seen from Fig. 2, the reaction barrier is 21 kcal mol^{-1}. So in the current simulations we only find these reaction trajectories when E_{coll} = 40 kcal mol^{-1}, and their contribution to the total reaction is also small, with values of only 0.4% in the ground-state case and 3% in the v_{HBr} = 1 case, and less than 1% for all the other mode-specific cases.

D. Scattering and initial attack angle distributions

Differential cross sections showing the scattering angle distributions of the HBr + C_2H_5 → Br + C_2H_6 reaction at different E_{coll} are shown in Fig. 7.

As can be seen in Fig. 7 the excitation of the HBr-stretching mode can clearly promote the forward scattering mechanism, so can the high collision energy, indicating the dominance of the direct stripping mechanism in these cases. At low collision energy with no excitation or excitation of any vibrational mode of C_2H_5, the forward scattering feature is less obvious. However, it is quite surprising that the DCS at E_{coll} = 1 kcal mol^{-1} shows more clearly a forward preference than E_{coll} = 5 kcal mol^{-1}, which may indicate a different mechanism at low E_{coll}. Nevertheless, this forward scattering is consistent with the significantly larger b_{max} value at low E_{coll} (see Fig. 5), because at large b stripping usually occurs resulting in forward scattering.

Normalized initial attack angle distributions for the HBr(v_{HBr} = 0, 1) + C_2H_5(v_x = 0, 1) → Br + C_2H_6 [x = 9, 5, 1, 10] reactions are plotted in Fig. 8. The reaction favors H-side attack over side-on HBr and the least-preferred Br-side approach, along with increasing collision energy, as expected, because an H–C bond forms in the abstraction process, but no clear mode-specificity is observed. The reaction favors side-on CH_3CH_2 attack over CH_2-side attack and the least-preferred CH_3-side approach, without significant mode-specificity. However, with increasing the collision energy, the pattern in the CH_3CH_2 attack angle is the opposite compared to HBr.

E. The post-reaction distribution of energy

Differential cross sections showing the distribution of the relative translational energy of the products at different E_{coll} are plotted in Fig. 9.

As shown in Fig. 9, no clear mode-specificity is observed at high collision energy. At E_{coll} = 1 kcal mol^{-1}, however, when the HBr-stretching mode is excited, the product clearly gains more relative translational energy. This is because the vibrational HBr-stretching energy transfers to translational energy after the H–Br bond is broken. When the excitation is in C_2H_5, the effect is opposite at E_{coll} = 1 kcal mol^{-1}.

The internal energy distributions of the product ethane, plotted in the upper panels of Fig. 10, feature clear mode-specificity with maxima shifting towards higher energies with nearly the value of the excess vibrational energy at low E_{coll}. At high E_{coll}, however, more collision energy is transferred into the vibrational and rotational degrees of freedom of ethane. Nevertheless, the internal energy excitations of the product ethane mainly come from the reaction energy. Vibrational energy distributions in the upper-middle panels of Fig. 10 confirm the above conclusion, but show a red shift compared to internal energy distribution, due to the fact that some of the vibrational energy is transferred into rotational energy, especially at high E_{coll} (lower-middle panels). No significant mode-specificity is observed for the rotational energy or the rotational quantum number distributions, as shown in the lower-middle and lower panels of Fig. 10.

IV. Conclusions

We have performed QCT simulations for the HBr + C_2H_5 reaction on a recently developed high-level *ab initio* full-dimensional spin–orbit-corrected PES by exciting five different vibrational modes of reactants at five collision energies. The effect of five normal-mode excitations on the reactivity, the mechanism, and the post-reaction energy flow is followed through a wide range of collision energies, and compared with the ground-state reaction. A substantial decrease of reaction probability for v_{HBr} = 1 reaction at low E_{coll}, caused by longer initial distance of the reactants is observed, whereas the initial distance does not affect the reactivity significantly at higher collision energies and for the ground-state reactants. All of the three reaction pathways are intensely promoted when the HBr-stretching mode is excited while no clear promotion is observed when excitation happens in C_2H_5. The promoting effect of the excitation in the HBr-stretching mode is found to be much more effective than translational enhancement, in contrast to the HBr + CH_3 reaction. Excitation of the HBr-stretching mode can clearly promote the forward scattering mechanism, so can the high collision energy, indicating the dominance of the direct stripping mechanism. At low collision energy with ground state or excitation of any vibrational mode of C_2H_5, the forward scattering feature is less obvious. The initial attack angle preference shows no significant mode-specificity; neither do the translational energy distributions at high collision energy. At E_{coll} = 1 kcal mol^{-1}, however, when the HBr-stretching mode is excited, the product clearly gains more relative translational energy. This is because the vibrational HBr-stretching energy transfers to translational energy after the H–Br bond is broken. However, it is interesting to see that when the excitation is in C_2H_5, the effect is the opposite. The internal energy distributions of the product ethane feature clear mode-specificity with maxima shifting towards higher energies with nearly the value of the excess vibrational energy at low E_{coll}. At high E_{coll} however, more collision energy is transferred into the vibrational and rotational degrees of freedom of ethane. Nevertheless, the internal energy excitations of the product ethane mainly come from the reaction energy. No significant mode-specificity is observed for rotational energy or rotational quantum number distributions. We hope that our work will inspire further experimental and theoretical studies on the mode-specificity of this reaction family, the new benchmark systems of polyatomic reaction dynamics.

Data availability

The data that support the findings of this study are available from the corresponding authors upon reasonable request.

Conflicts of interest

There are no conflicts to declare.

Acknowledgements

This work was supported by the National Research, Development and Innovation Office – NKFIH, K-125317; the Ministry of Human Capacities, Hungary grant 20391-3/2018/FEKUSTRAT; Project no. TKP2021-NVA-19, provided by the Ministry of Innovation and Technology of Hungary from the National Research, Development and Innovation Fund, financed under the TKP2021-NVA funding scheme; and the Momentum (Lendület) Program of the Hungarian Academy of Sciences. We thank Viktor Tajti for discussions about the mode-specific initial condition setups.

References

1 D. J. Donaldson and S. Leone, *J. Phys. Chem.*, 1986, **90**, 936.
2 I. J. Russell, J. A. Seetula and D. Gutman, *J. Am. Chem. Soc.*, 1988, **110**, 3092.
3 J. M. Nicovich, C. A. Van Dijk, K. D. Kreutter and P. H. Wine, *J. Phys. Chem.*, 1991, **95**, 9890.
4 P. W. Seakins, M. J. Pilling, J. T. Niiranen, D. Gutman and L. N. Krasnoperov, *J. Phys. Chem.*, 1992, **96**, 9847.
5 J. A. Seetula, *J. Chem. Soc., Faraday Trans.*, 1998, **94**, 891.
6 J. A. Seetula, *Phys. Chem. Chem. Phys.*, 2002, **4**, 455.
7 L. N. Krasnoperov and K. Mehta, *J. Phys. Chem. A*, 1999, **103**, 8008.
8 N. Leplat, A. Wokaun and M. J. Rossi, *J. Phys. Chem. A*, 2013, **117**, 11383.
9 N. Leplat and M. J. Rossi, *J. Phys. Chem. A*, 2014, **118**(28), 5135.
10 Y. Chen, E. Tschuikow-Roux and A. Rauk, *J. Phys. Chem.*, 1991, **95**, 9832.
11 Y. Chen, E. Tschuikow-Roux and A. Rauk, *J. Phys. Chem.*, 1991, **95**, 9900.
12 H. Yu and G. Nyman, *J. Phys. Chem. A*, 2001, **105**, 2240.
13 J. Espinosa-Garcia, *J. Chem. Phys.*, 2002, **117**, 2076.
14 L. Sheng, Z.-S. Li, J.-Y. Liu and C.-C. Sun, *J. Chem. Phys.*, 2003, **119**, 10585.
15 L. N. Krasnoperov, J. Peng and P. Marshall, *J. Phys. Chem. A*, 2006, **110**, 3110.
16 Y. Wang, L. Poing, H. Song and M. Yang, *Theor. Chem. Acc.*, 2017, **136**, 59.
17 G. Czakó, *J. Chem. Phys.*, 2013, **138**, 134301.
18 S. Góger, P. Szabó, G. Czakó and G. Lendvay, *Energy Fuels*, 2018, **32**, 10100.
19 D. Gao, X. Xin, D. Wang, P. Szabó and G. Lendvay, *Phys. Chem. Chem. Phys.*, 2022, **24**, 10548.
20 Y. H. Chen and E. Tschuikow-Roux, *J. Phys. Chem.*, 1993, **97**, 3742.
21 J. A. Seetula, *Phys. Chem. Chem. Phys.*, 2000, **2**, 3807.
22 L. Sheng, Z. S. Li, J. Y. Liu, J. F. Xiao and C. C. Sun, *J. Comput. Chem.*, 2004, **25**, 423.
23 D. M. Golden, J. P. Peng, A. Goumri, J. Yuan and P. Marshall, *J. Phys. Chem. A*, 2012, **116**, 5847.
24 D. Papp, B. Gruber and G. Czakó, *Phys. Chem. Chem. Phys.*, 2019, **21**, 396.
25 C. Yin, V. Tajti and G. Czakó, *Phys. Chem. Chem. Phys.*, 2022, **24**, 24784.
26 T. Győri and G. Czakó, *J. Chem. Phys.*, 2022, **156**, 071101.
27 K. A. Peterson, D. Figgen, E. Goll, H. Stoll and M. Dolg, *J. Chem. Phys.*, 2003, **119**, 11113.
28 H.-J. Werner and P. J. Knowles, *J. Chem. Phys.*, 1988, **89**, 5803.
29 S. R. Langhoff and E. R. Davidson, *Int. J. Quantum Chem.*, 1974, **8**, 61.
30 A. Berning, M. Schweizer, H.-J. Werner, P. J. Knowles and P. Palmieri, *Mol. Phys.*, 2000, **98**, 1823.
31 Z. Xie and J. M. Bowman, *J. Chem. Theory Comput.*, 2010, **6**, 26.
32 W. L. Hase, *Encyclopedia of Computational Chemistry*, Wiley, New York, 1998, pp. 399–407.
33 D. Papp, J. Li, H. Guo and G. Czakó, *J. Chem. Phys.*, 2021, **155**, 114303.